Chemosphere 287 (2022) 132271

Contents lists available at ScienceDirect

Chemosphere

journal homepage: www.elsevier.com/locate/chemosphere

Novel biogenic silver and gold nanoparticles for multifunctional applications: Green synthesis, catalytic and antibacterial activity, and colorimetric detection of Fe(III) ions

Thi Hong Anh Nguyen [a], Van-Cuong Nguyen [b], Thi Nhu Huynh Phan [b], Van Thuan Le [c,d,*], Yasser Vasseghian [e,***], Mikhail Alexandrovich Trubitsyn [f], Anh-Tien Nguyen [g], Tan Phat Chau [h], Van-Dat Doan [b,**]

[a] Faculty of Chemical Engineering, Ho Chi Minh City University of Food Industry, 140 Le Trong Tan, Ho Chi Minh City, 70000, Viet Nam
[b] Faculty of Chemical Engineering, Industrial University of Ho Chi Minh City, Ho Chi Minh City, 70000, Viet Nam
[c] Center for Advanced Chemistry, Institute of Research and Development, Duy Tan University, 03 Quang Trung, Da Nang, 550000, Viet Nam
[d] The Faculty of Environment and Natural Sciences, Duy Tan University, 03 Quang Trung, Da Nang, 550000, Viet Nam
[e] Department of Chemical Engineering, Quchan University of Technology, Quchan, Iran
[f] Belgorod State National Research University, 85 Pobeda, Belgorod City, 308015, Russia
[g] Faculty of Chemistry, Ho Chi Minh City University of Education, 280 An Duong Vuong, Ho Chi Minh City, 70000, Viet Nam
[h] Institute of Applied Science & Technology, Van Lang University, Ho Chi Minh City, 700000, Viet Nam

HIGHLIGHTS

- Biogenic AgNPs and AuNPs were prepared using *Ganoderma lucidum* extract.
- Both MNPs possessed excellent catalytic activity for the reduction of 4-nitrophenol.
- AgNPs showed strong antibacterial activity against several bacterial strains.
- The AgNPs-based probe can accurately determine Fe^{3+} in water with LOD of 1.85 nM.

GRAPHICAL ABSTRACT

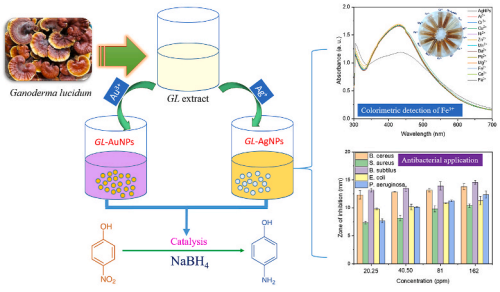

ARTICLE INFO

Handling Editor: Hafiz M.N.Iqbal

Keywords:
Ganoderma lucidum
Green synthesis
Metallic nanoparticles
4-Nitrophenol reduction

ABSTRACT

In this study, novel biogenic silver (AgNPs) and gold nanoparticles (AuNPs) were developed using a green approach with *Ganoderma lucidum* (GL) extract. The optimization of synthesis conditions for the best outcomes was conducted. The prepared materials were characterized and their applicability in catalysis, antibacterial and chemical sensing was comprehensively evaluated. The GL-AgNPs crystals were formed in a spherical shape with an average diameter of 50 nm, while GL-AuNPs exhibited multi-shaped structures with sizes ranging from 15 to 40 nm. As a catalyst, the synthesized nanoparticles showed excellent catalytic activity (>98% in 9 min) and

* Corresponding author. Center for Advanced Chemistry, Institute of Research and Development, Duy Tan University, 03 Quang Trung, Da Nang, 550000. Viet Nam.
** Corresponding author.
*** Corresponding author.
E-mail addresses: levanthuan3@duytan.edu.vn (V.T. Le), y.vasseghian@qiet.ac.ir (Y. Vasseghian), doanvandat@iuh.edu.vn (V.-D. Doan).

https://doi.org/10.1016/j.chemosphere.2021.132271
Received 31 July 2021; Received in revised form 1 September 2021; Accepted 15 September 2021
Available online 16 September 2021

Antibacterial activity
Colorimetric detection

reusability (>95% after five recycles) in converting 4-nitrophenol to 4-aminophenol. As an antimicrobial agent, GL-AuNPs were low effective in inhibiting the growth of bacteria, while GL-AgNPs expressed strong antibacterial activity against all the tested strains. The highest growth inhibition activity of GL-AgNPs was observed against *B. subtilis* (14.58 ± 0.35 mm), followed by *B. cereus* (13.8 ± 0.52 mm), *P. aeruginosa* (12.38 ± 0.64 mm), *E. coli* (11.3 ± 0.72 mm), and *S. aureus* (10.41 ± 0.31 mm). Besides, GL-AgNPs also demonstrated high selectivity and sensitivity in the colorimetric detection of Fe^{3+} in aqueous solution with a detection limit of 1.85 nM. Due to the suitable thickness of the protective organic layer and the appropriate particle size, GL-AgNPs validated the triple role as a high-performance catalyst, antimicrobial agent, and nanosensor for environmental monitoring and remediation.

1. Introduction

The advent of nanotechnology in recent decades has made an enormous leap forward in materials science by creating nanostructured materials with unique physicochemical properties. Nanomaterials exhibit novel or improved properties that may be completely different from those of bulk materials due to their superior surface-area-to-volume ratio and the possible appearance of quantum effects at the nanoscale (Soni et al., 2021). In particular, noble metal nanoparticles (MNPs) such as silver (AgNPs) and gold nanoparticles (AuNPs) have recently received great attention from the scientific world owing to their attractive features of excellent catalytic and antimicrobial activities, biocompatibility, high photo-electrochemical activity, chemical inertness, and simple synthesis (Saravanan et al., 2021). With these distinctive properties, MNPs have become useful in many fields such as medicine, agriculture, electronics, bioengineering, catalysis, biosensors, water treatment, and controlling microorganism development (Le et al., 2021b; Saravanan et al., 2021).

In the past few years, MNPs have been intensively applied as a remarkable catalyst for the reduction of toxic nitrophenols with sodium borohydride ($NaBH_4$) due to their larger specific areas and high electrical conductivity (My-Thao Nguyen et al., 2021). It is a known fact that the reduction of nitrophenols by $NaBH_4$ without a catalyst is kinetically unfavourable by reason of the high kinetic barrier between 4-nitrophenolate ($C_6H_4NO_3^-$) and borohydride (BH_4^-) (Gangapuram et al., 2018). However, the presence of MNPs can promote the decomposition of $NaBH_4$ to BH_4^- ions, and moreover, MNPs can act as a mediator for the electron relay between the donor (BH_4^-) and acceptor (nitrophenols), improving the conversion of nitrophenols into aminophenols (Grzeschik et al., 2020). The significant enhancement of nitrophenols reduction with the participation of AgNPs and AuNPs catalysts has been demonstrated in many studies (Soni et al., 2021; T. T. Vo et al., 2020). It should be noticed that the conversion of nitrophenols into aminophenols provides a great environmental and economic benefits because aminophenol compounds are widely used in producing several important pharmaceuticals, dyes, polymers, cosmetics, and agrochemicals (Berahim et al., 2018).

One of the most prominent practical applications of MNPs is their use as an effective antibacterial agent (Alavi and Rai, 2019). The small size and larger surface area of MNPs can enhance the binding strength of the bacterial membrane with the nanoparticles, causing opsonization of the bacterial membrane. The adhesion of MNPs on the bacterial membrane can lead to the increased permeability, resulting in leakage of cytoplasmic substances and cell death *via* the Donnan effect (Nayak et al., 2018). Although until now the exact mechanism for the antimicrobial effect of MNPs is not fully explored, their superior antibacterial ability is undisputed.

Recently, there has been an increasing interest in the use of AgNPs and AuNPs as nanosensors for colorimetric detection of target metal ions in aqueous solutions thanks to their high surface reactivity, tunable size, and a high degree of functionalization (Buledi et al., 2020). Many studies have shown that using MNPs-based sensors offers great advantages such as the high sensitivity and selectivity, cost-effective, simple operations, and rapid analysis (Ho et al., 2021; Le et al., 2021c). Moreover, these assays can also provide the ability to detect heavy metal ions with the naked-eye inspection through color changes without expensive apparatus compared with other methods. Up to now, many sensors based on AuNPs and AgNPs have been developed for the determination of toxic metal ions. For instance, Modrzejewska-Sikorska et al. designed the chemical probes from lignosulfonate stabilized AgNPs and AuNPs and successfully applied them for sensing Cu^{2+}, Pb^{2+}, Co^{2+}, Cd^{2+}, and Ni^{2+} ions in model aqueous solutions. The study observed the color change, surface plasmon resonance (SPR) peak shift, and aggregation of the MNPs solution when incubated with metal ions, which served as the main principle of colorimetric detection (Modrzejewska-Sikorska and Konował, 2020). Annadhasan and co-workers reported the high-sensitivity colorimetric detection of Hg^{2+} and Mn^{2+} ions using L-tyrosine-stabilized AgNPs with a limit of detection (LOD) of 16 nM for both ions. Lately, Le et al. reported the colorimetric sensor fabricated from *Siraitia grosvenorii* extract AuNPs, which could accurately detect Pb^{2+} ions in a linear concentration range of 0–1000 μM with LOD of 0.018 μM (Le et al., 2021c).

Currently, MNPs have been extensively produced to meet their growing demand for several important areas of application. There are many approaches available for MNPs synthesis, including physical, chemical, and biological methods. However, physical and chemical synthesis has remarkable disadvantages, such as the utilization of hazardous chemicals, energy-consuming, strict preparation conditions, and high cost (Saravanan et al., 2021). Hence, the synthesis of MNPs using biological materials is preferred because it is simple, environmentally friendly, cost-effective, and does not involve any toxic substances. Several plants like *Eriobotrya japonica* (thunb.) (Yu et al., 2019), *Litsea cubeba* (Doan et al., 2020b), *Bauhinia variegate* (Uzunoğlu et al., 2020), *Lactuca indica* (T.-T. Vo et al., 2020), *Siraitia grosvenorii* (Le et al., 2021c), ect., have been used for the MNPs fabrication. Notably, MNPs produced by plant-mediated synthesis are reported to have enhanced catalytic and antibacterial activity and high stability owing to the presence of an organic layer capped around nanoparticles. Also, the variety in phytochemicals of various plants can result in different properties of the prepared MNPs (Nayak et al., 2018). Therefore, at present new plants are still being explored to synthesize MNPs.

In this study, we the first time utilized *Ganoderma lucidum* (GL) mushroom, an edible Basidiomycetes fungus of the family Polyporaceae grown on dead reishi in primary forests, to fabricate AuNPs and AgNPs. GL mushroom is well known as a traditional medicine of Asian countries; it is often used to enhance the immune system, prevent and treat various diseases due to its antioxidant, antibacterial, anti-inflammatory, and anticancer (Karst, 2020). Phytochemical analysis revealed that GL is rich in steroids, polysaccharides, alkaloids, triterpenoids, sesquiterpenoids, and meroterpenoids, which can act as reducing and stabilizing agents in the MNPs synthesis process (Al-Ansari et al., 2020). Furthermore, using medicinal plants like GL mushroom for synthesis will increase the biocompatibility and biological activity of the prepared MNPs. The synthesis parameters, including metal ion concentration, reaction time and temperature, were optimized to select the best synthesis condition. The MNPs produced at optimized conditions (denoted as GL-AgNPs and GL-AuNPs) were characterized by prevailing instrumentation techniques and then applied for the reduction of 4-nitrophenol (4-NP),

colorimetric detection of Fe^{3+}, and antimicrobial activity against *B. subtilis*, *S. aureus, B. cereus, E. coli,* and *P. aeruginosa* bacteria.

2. Experimental section

2.1. Materials

G. lucidum mushroom was picked from natural forest in Tien Phuoc district, Quang Nam province, Vietnam. Silver nitrate ($AgNO_3$, 99.85%), gold(III) chloride ($AuCl_3$, 99%), sodium borohydride ($NaBH_4$, ≥98.0%), and 4- nitrophenol (4-NP, $O_2NC_6H_4OH$, ≥ 99%) were acquired from ACROS Organics (Belgium). All metal salts, including $AlCl_3$ (99%), $CrCl_3.6H_3O$ (99%), $CuCl_2.2H_2O$ (≥99%), $NiCl_2.6H_2O$ (99.9%), $ZnCl_2$ (≥98%), $MnCl_2$ (≥99%), $BaCl_2.2H_2O$ (≥99%), $MgCl_2.6H_2O$ (≥99%), $CaCl_2$ (≥97%), $FeCl_2.4H_2O$ (≥99%), $FeCl_3.6H_2O$ (≥99%), and $Pb(NO_3)_2$ (≥99%), were provided by Merck (Singapore). All used bacterial strains (*B. subtilis*, *S. aureus, B. cereus, E. coli,* and *P. aeruginosa*) were attained from the Department of Biotechnology, Institute of Food and Biotechnology, Industrial University of Ho Chi Minh City, Vietnam.

2.2. Preparation of GL extract

The collected fresh GL mushrooms were washed with distilled water several times, dried until the moisture content was about 10%, and then ground into a fine powder. The GL powder (2 g) was boiled with 200 mL of distilled water for 1 h, and after that, cooled naturally to room temperature. The resulting extract was filtered through Whatman filter paper No. 1 and stored in a refrigerator (2–8 °C). It is recommended to use the fresh GL extract (no more than 5 days after extraction) for synthesizing MNPs.

2.3. Biosynthesis of GL-MNPs

The biosynthesis of GL-MNPs was performed by mixing the GL extract and metal ion solution (Ag^+ or Au^{3+}) in a volume ratio of 1:1 under different metal ion concentrations (0.25–3.0 mM), reaction time (15–105 min), and temperatures (60–100 °C). To determine the optimal synthesis condition, the effects of experimental parameters on the formation of AgNPs and AuNPs were investigated by altering survey preparative parameters while fixing the other circumstances. The detailed experimental conditions are summarized in Table S1 (Supporting Material). The formation of AgNPs and AuNPs was monitored and confirmed by the appearance of the characteristic UV–Vis SPR peaks around 420 and 540 nm, respectively (Doan et al., 2020a). The best conditions were established based on two main factors of the high MNPs concentration and stability of the colloidal solutions obtained. According to the results of the optimization study (Fig. S1), the suitable metal ions concentration, reaction time, and temperature for the synthesis of GL-AgNPs and GL-AuNPs were selected to be 2.5 mM, 90 min, and 100 °C for GL-AgNPs, and 1.5 mM, 40 min, and 70 °C, respectively.

The optimized MNPs colloidal solutions were further applied directly for the catalytic reduction of 4-NP, antibacterial testing, and determination of Fe^{3+} ions in aqueous solution. The dry MNPs powder collected by ultracentrifugation was further used for characterization.

2.4. Apparatus

UV–Vis measurements were carried out on a Cary 60 UV–Vis spectrophotometer (Agilent, USA). The transmission electron microscopy (TEM) and Field emission scanning electron microscopy (FE-SEM) images were taken on Tecnai G2 20 S-TWIN and Hitachi S-4800 (Japan) instruments, respectively. The X-ray diffraction (XRD) patterns were recorded by a Shimadzu 6100 X-ray diffractometer (Japan) operated at a current of 30 mA and voltage of 40 kV using CuKα radiation (λ = 1.5406 Å). The Fourier transform infrared (FTIR) analysis was conducted on a Bruker Tensor 27 spectrometer (Germany). A Horiba SZ-100 nanoparticle size and zeta potential analyzer (Japan) was used to determine the dynamic light scattering (DLS) particle size distribution and zeta potential of MNPs samples. The chemical elements present in the samples and their mapping were examined by energy-dispersive X-ray spectroscopy (EDX) using an EMAX Energy EX-400 analyser (Horiba, Japan).

2.5. Catalytic activity evaluation

The reduction reaction of 4-NP with $NaBH_4$ was used for evaluating the catalytic activity of the produced MNPs. The catalytic reaction was carried out in a 10-mm path length quartz cuvette (3 mL) with 2.5 mL of 0.5 mM 4-NP, 0.5 mL of 0.5 M $NaBH_4$, and 3 μL of MNPs solutions at room temperature. The change of concentration of 4-NP with time during the catalytic process was monitored by a UV–Vis spectrophotometer. At the end of the reaction, the MNPs catalysts were recovered by centrifugation, washed with alcohol and distilled water, and dried for subsequent reuse cycles. The conversion percentage was calculated by Eq. (1) (Doan et al., 2021).

$$Conversion(\%) = \frac{A_0 - A_t}{A_0} x100\% \quad (1)$$

where A_o and A_t are the absorbance of the 4-NP solution at time $t = 0$ and $t = t$, respectively.

2.6. Colorimetric assay application

The colorimetric sensing application of GL-MNPs was investigated with several metal ions (Al^{3+}, Cr^{3+}, Fe^{3+}, Mn^{2+}, Zn^{2+}, Ni^{2+}, Mg^{2+}, Pb^{2+}, Ba^{2+}, Ca^{2+}, Cu^{2+}, and Fe^{2+}) by the following procedures. 1 mL of the GL-MNPs solution was mixed with 2 mL of each metal ion (20 nM) at room temperature and incubated for 5 min. After that, the UV–Vis spectra of the mixture were recorded, and the change in color of the GL-MNPs solution was observed. For quantitative sensing of Fe^{3+}, various concentrations of Fe^{3+} (0.1–500 nM, 2 mL) was added to the GL-MNPs solution (1 mL), the absorbance intensity of the SPR band of the incubated mixture was then measured to establish the detectable linear range. The applicability of the proposed probe was tested with tap water spiked with Fe^{3+} standard solutions in the range of 50–500 nM. The accuracy of the developed assay was evaluated through the recovery values and compared with the atomic absorption spectroscopy (AAS) method.

2.7. Antibacterial activity tests

The antibacterial activity of the prepared MNPs was determined by the agar disk diffusion method (Doan et al., 2020a). Five bacterial strains, including two Gram-negative bacteria (*P. aeruginosa* and *E. Coli*) and three Gram-positive bacteria (*B. subtilis, S. aureus*, and *B. cereus*) were used for the testing experiments. The GL extract (50 μL) and gentamicin antibiotic discs was utilized as negative and positive controls for the purpose of comparison, respectively. The fresh chosen bacterial cultures (100 μL, 10^5–10^6 CFU/mL) were spread on the Muller Hinton Agar plates using a sterile glass swab. The 6-mm diameter wells were then punched in agar plates by sterile gel puncture. Afterwards, 50 μL of MNPs with concentrations of 20–160 ppm and control samples were poured in the prepared wells. The inoculated plates were incubated at 37 °C for 24 h. Upon completion of incubation, zones of inhibition were measured to assess antibacterial activity.

3. Results and discussion

3.1. Characterization of GL-MNPs

The morphology of the synthesized MNPs in the colloidal and

powder forms was examined by TEM (Fig. 1a and b) and FE-SEM (Fig. 1 c and d) images, respectively. As shown in the TEM images, the GL-AgNPs crystals were presented in a spherical shape with an average diameter of about 50 nm (Fig. 1a), while GL-AuNPs exhibited multi-shaped structures including triangular, spherical, hexagonal, pentagonal, rhombus, and nanorods with sizes ranging from 15 to 40 nm (Fig. 1b). A similar morphology was also obtained when synthesizing AgNPs and AuNPs by the extract from *Crinum latifolium* leaf (Vo et al., 2019). It is noteworthy that MNPs were well separated from each other, which was probably supported by the organic layer surrounding the nanoparticles. In powder form, MNPs were mostly spherically shaped and agglomerated into clusters, as shown in Fig. 1c and d. However, the detached MNPs with an average size of about 50 nm could be observed, indicating no change in particle size in the powder state. The chemical composition of the biosynthesized MNPs was confirmed by the EDX analysis. The EDX spectra of GL-AgNPs (Fig. 1e) and GL-AuNPs (Fig. 1f) revealed the presence of metallic silver (2.63, 2.98, and 3.15 keV) and gold (1.67, 2.13, 2.40, and 9.71 keV). Along with this, the peaks located at 0.28 and 0.53 keV characteristic for C and O elements were also found in both EDX spectra. The appearance of these elements in the prepared samples was derived from biomolecules stabilizing MNPs. This provided evidence for the organic capping layer. The EDX quantitative analysis

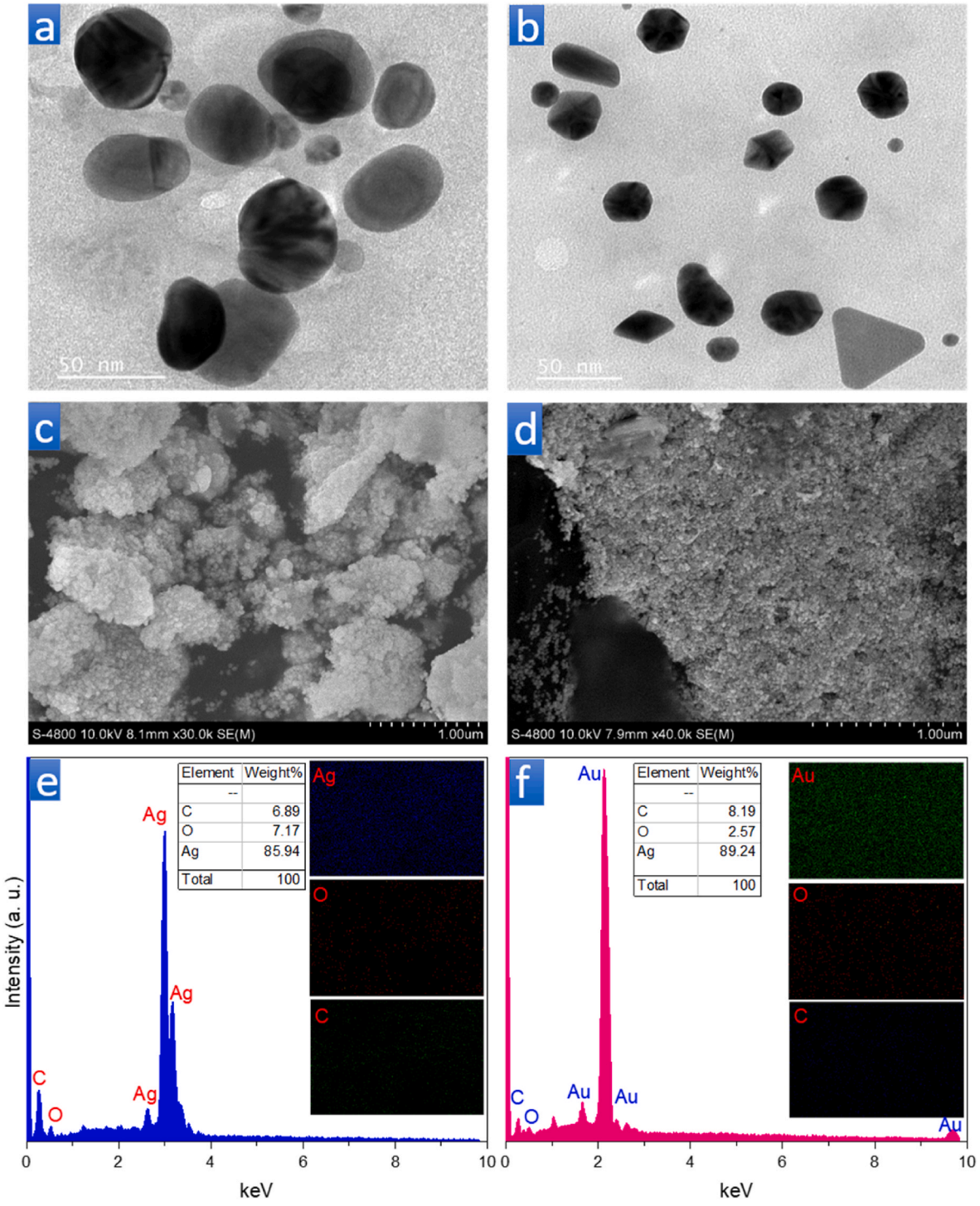

Fig. 1. TEM (a & b), FE-SEM (c & d) images, EDX spectra and element mapping (e & f) of GL-AgNPs (a, c, e) and GL-AuNPs (b, d, f).

indicated that Ag and Au exhibited the highest weight percentage (>85%) in the GL-AgNPs and GL-AuNPs samples, respectively. Other elements were in very small amounts (<10%) (see the tables inserted in Fig. 1e and f). The same result was also obtained for *Tephrosia purpurea* leaf extract AgNPs and AuNPs (Ajitha et al., 2014). Furthermore, the distribution of the elements on the MNPs surface was monitored by EDX element mapping, as depicted in the insets of Fig. 1e and f. The results showed the uniform distribution of the elements on the biogenic MNPs.

The XRD analysis was conducted to elucidate the crystalline nature and phase purity of as-prepared materials. The GL-AgNPs and GL-AuNPs gave typical XRD patterns (Fig. 2a) for AgNPs and AuNPs synthesized using plant extracts, which can be found in several reported works (Doan et al., 2020a; Le et al., 2021a, 2021c). Four intensive peaks characteristic for (111), (200), (220), and (311) planes of the face-centered cubic structure of silver and gold could be detected at 2Θ of 38.2°, 43.3°, 64.4°, and 77.4°, respectively. The broad diffraction peak at 2Θ of 24° was assigned to amorphous carbon derived from the organic layer covering MNPs. The fine crystalline nature of the formed MNPs was established by narrow and sharp diffraction peaks. Compared with GL-AgNPs, the GL-AuNPs sample possessed higher and sharper diffraction peaks, possibly due to their smaller crystallite size. No other strange peaks were found, demonstrating the high purity of the synthesized materials.

The FTIR measurements were performed to identify functional groups responsible for reducing and stabilizing of MNPs. Fig. 2b depicts the FTIR spectra of GL extract, GL-AgNPs, and GL-AuNPs. It can be seen that the FITR spectra of the biosynthesized MNPs samples almost coincided with that of the GL extract, proving the existence of GL phytoconstituents on the surface of MNPs. The bands around 620, 1558, 1402 cm^{-1} were assigned to the C – H stretch, symmetrical and asymmetrical stretching vibrations of C = C bonds from aromatic rings, respectively. The C–O–C stretching vibration of polysaccharides was characterized by the peaks at 1045 and 1115 cm^{-1} (Dao et al., 2020). The occurrence of the small peak at 1735 cm^{-1} indicated the presence of the C = O stretching from ketones, esters, and carboxyl groups present in GL extract. The C–H stretching vibrations of $–CH_3$ and $–CH_2$ groups were detected at 2920 and 2849, respectively. The broad absorption band around 3381 cm^{-1} associated with O–H stretching of hydroxyl groups, which were believed to be a major contributing factor in the reduction of metal ions to MNPs. Indeed, several studies have reported that hydroxyl groups are able to reduce Ag^{+} and Au^{3+} to AgNPs and AuNPs by transferring electrons to them (Behzad et al., 2021; Le et al., 2021c; Seku et al., 2018).

As mentioned above, phytoconstituents of GL extract not only act as reducing agents but also play an important role in stabilizing the produced MNPs. After reduction, the GL biomolecules adsorbed on the MNPs surface, creating an organic envelope that prevents agglomeration of the particles. The thickness of this protective organic layer often has certain effects on the properties of the prepared materials. A too thick organic layer will prevent physical contact of the metal surface with the object, resulting in the decrease of catalytic and antibacterial activities. The size of this layer can be estimated relatively by determining the diameter of MNPs in aqueous solution and comparing with their crystal size obtained by TEM. The hydrodynamic diameter of MNPs was measured by the DLS technology and given in Fig. 2c&d. The DLS diagrams revealed that GL-AgNPs exhibited a particle size distribution between 25 and 150 nm with an average diameter of 55 nm (Fig. 2c), while the hydrodynamic size of GL-AuNPs was distributed over a wider

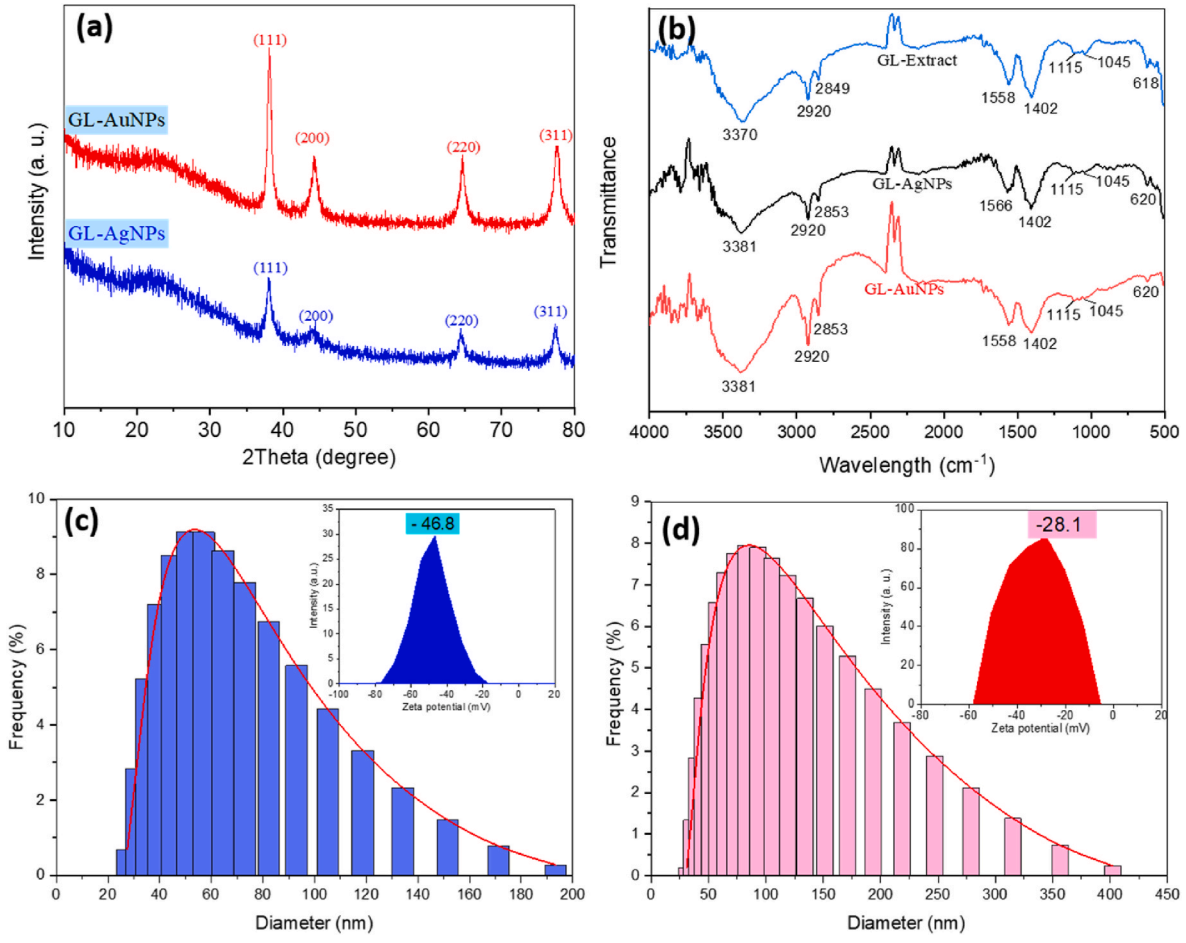

Fig. 2. XRD patterns (a), FITR spectra (b), and DLS diagrams and zeta potentials of GL-AgNPs (c) and GL-AuNPs (d).

range from 25 to 400 nm with an average value centered at 80 nm (Fig. 2d). It can be noticed that the MNPs sizes obtained by DLS were larger than that from the TEM images; this was because that the TEM measurement gave the bare size of the crystals, while the DLS technique offered the hydrodynamic size involving the solvation and organic layers. Furthermore, the crystal size of GL-AgNPs was larger than that of GL-AuNPs, but their hydrodynamic size was opposite, suggesting the thicker protective organic layer of AuNPs compared with AgNPs. This phenomenon could be related to the difference in charge between Ag^{+} and Au^{3+}. Due to higher positive charge, AuNPs could adsorb more biomolecules with negatively charged oxygen-containing functional groups (e. g., –OH and –COOH) through electrostatic attraction. Another possible cause was that the concentration of Au^{3+} (1.5 mM) used for synthesis was lower than that of Ag^{+} (2.5 mM), resulting in a higher excess of phytoconstituents on the AuNPs surface.

The stability of a colloidal solution is one of the important factors determining its applicability. Agglomeration of particles is considered the main cause of precipitation, leading to a decrease in the stability of the MNPs solution. For plant-mediated synthesized MNPs, their agglomeration ability can be empirically predicted through the zeta potential. The high absolute value of the zeta potential ensures the good stability of the distributed system. As displayed in the insets of Fig. 2c

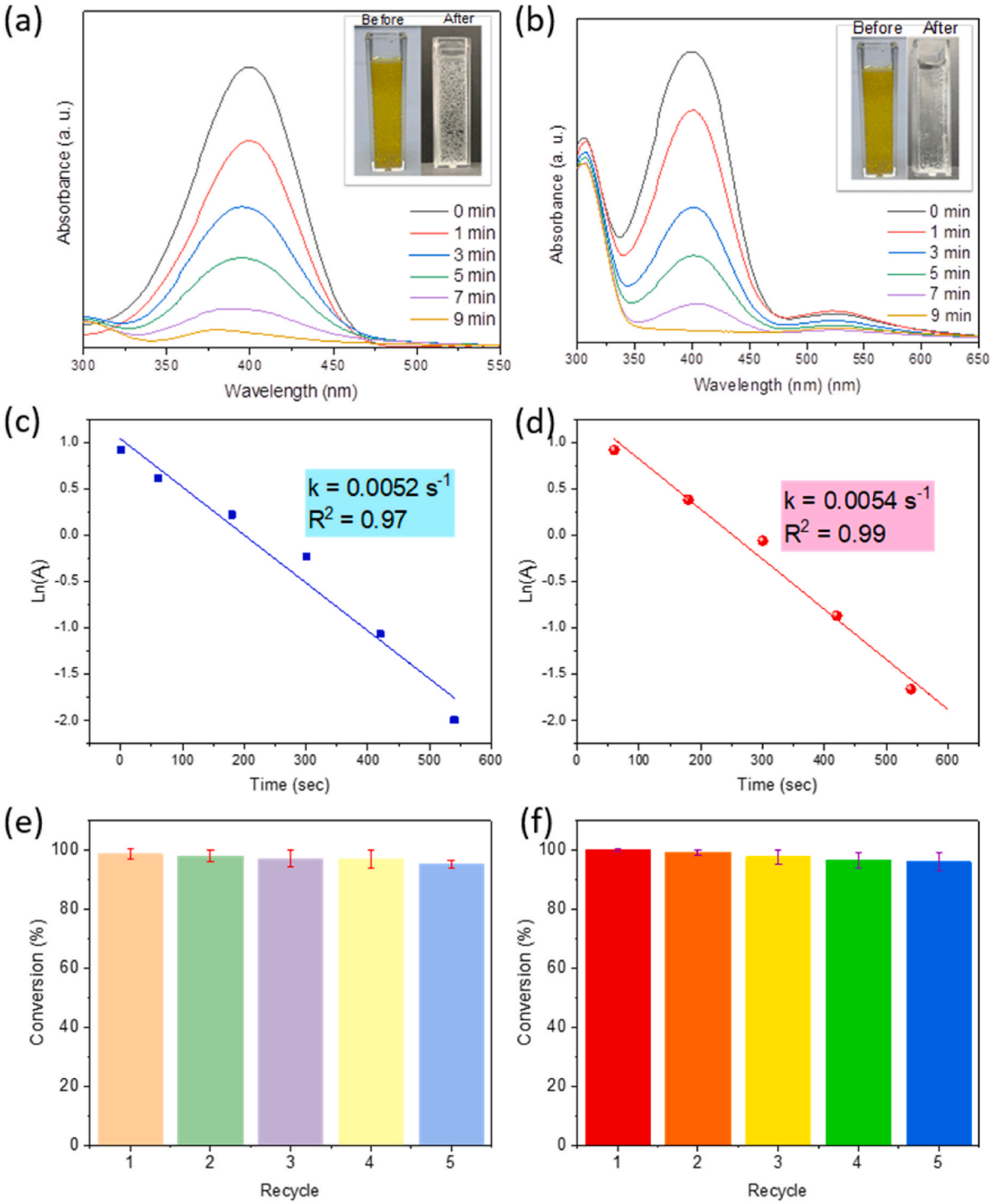

Fig. 3. UV–Vis spectra, plot of $Ln(A_t)$ versus time, and recycling for reduction of 4-NP by GL-AgNPs (a, c, e) and GL-AuNPs (b, d, f).

and d, the zeta potential of the GL-AgNPs and GL-AuNPs solutions in neutral conditions was −46.8 and −28.1 eV, respectively. These values were remarkably higher than that of AgNPs (−19.9 mV) and AuNPs (−20.8 mV) produced using *Crinum latifolium* leaf extract (Vo et al., 2019). The large absolute zeta potentials of GL-MNPs were a clear indication of the highly stable dispersion of the prepared colloidal solutions. The negative surface charge of GL-MNPs can be derived from the negative charge of the functional groups (–OH and –COOH) of the protective organic layer. The lower zeta potential of GL-AuNPs in comparison with GL-AgNPs could be related to the higher positive charge of Au^{3+}, which exhibited larger compensation towards the negatively charged capping layer (Behzad et al., 2021).

3.2. Catalytic activity

The catalytic activity of the produce MNPs was investigated using the reduction of 4-NP by $NaBH_4$ reductant as a model reaction. 4-NP was chosen as the subject of this study because it is one of the most common nitrophenols widely used for fabricating fertilizers, dyes, explosives, pesticides, and rubber. Unfortunately, 4-NP with aromatic structure displays high toxicity, non-biodegradability, carcinogenicity, and high stability in the environment; especially, it can damage the central nervous system and vital organs of humans and animals when exposed (Xu et al., 2020). The detailed mechanism of the reduction of 4-NP to 4-AP with the presence of $NaBH_4$ and MNPs has been reported in many previously published works (Albukhari et al., 2019; Le et al., 2021b; Shimoga et al., 2020). Fig. 3a and b show the UV–Vis spectra of the reaction mixture during reduction by GL-AgNPs and GL-AuNPs, respectively. After mixing with $NaBH_4$, 4-NP was deprotonated to form 4-nitrophenolate ($C_6H_4NO_3^-$) ions under basic conditions, which gave a maximum absorption peak at around 400 nm. The control experiment was also conducted in this study, showed that no significant reduction has been observed in the absence of the catalyst (Fig. S2.), as reported in several studies (Hassan et al., 2018; Rarima and Unnikrishnan, 2020). From Fig. 3a and b, it can be noticed that 4-nitrophenolate ions were easily and rapidly reduced into 4-AP with the participation of the small amount of MNPs, as evidenced by the quick decrease in the intensity of the peak at 400 nm. The conversion calculated for GL-AgNPs and GL-AuNPs achieved 98.4% and 100% within 9 min, respectively. The observed higher catalytic performance of GL-AuNPs compared with GL-AgNPs could be due to their smaller crystal sizes, which provided a larger surface area. As determined above, GL-AuNPs exhibited higher hydrodynamic size and smaller crystal size but possessed higher catalytic activity, proving that the thickness of the organic layer protecting the MNPs had no effect on their catalytic ability. This can be attributed to the fact that the organic layer of MNPs in aqueous solution was stretched by water molecules through hydrogen bonding, whereby small sized BH_4^- and 4-phenolate ions could easily pass through it and adsorb on the MNPs surface.

The catalytic activity of MNPs can be evaluated through the rate constant (k, s^{-1}) of the reduction reaction. In this study, the pseudo-first-order model $\ln(A_t) = -kt + \ln(A_o)$ (Eq. (2)) was applied to describe the reaction kinetics because the reduction of 4-NP was carried out with a large excess of $NaBH_4$, so the reaction rate depended almost exclusively on the 4-NP concentration (Doan et al., 2020b). Fig. 3c and d displays the plots of $\ln(A_t)$ versus time for the reduction reaction of 4-NP using GL-AgNPs and GL-AuNPs, respectively. The linear relationship with high correlation coefficients (R^2 = 0.97–0.99) confirmed the pseudo-first-order kinetic behavior of the catalytic reaction. The calculated rate constants for GL-AgNPs and GL-AuNPs were 0.0052 and 0.0054 s^{-1}, respectively. Compared with AgNPs and AuNPs prepared from *Limnophila rugosa* (Le et al., 2021a), *Crinum latifolium* (Vo et al., 2019), and *Codonopsis pilosula* (Doan et al., 2020a) extracts, both GL-AgNPs and GL-AuNPs exhibited superior catalytic activity.

The recycling test was conducted to elucidate the long-term applicability of the catalysts. As depicted in Fig. 3e and f, the catalytic efficiency of GL-MNPs toward 4-NP decreased slightly with increasing recycle number. This may be related to the loss of the catalyst during recovery and the inactivation of the catalyst sites due to the adsorption of by-products (Thi Thanh Nhi et al., 2020). In addition, the particle agglomeration after centrifugation, leading to a decrease in specific surface area, was also a reason of the performance loss. However, the catalyst materials still maintained over 95% conversion after five consecutive reuses, demonstrating their high stability.

3.3. Detection of Fe^{3+}

Nowadays, the presence of metal ions in wastewater and groundwater has been increasingly detected due to the rapid development of industries such as mining, metallurgy, plating, and chemical production (Ho et al., 2021). Delays in the detection and quantification of these pollutants can cause several environmental and health problems because they have different toxicological effects even at low concentrations. For instance, consuming too much iron ions from foods and drinks can cause hemoglobinopathy, which can lead to damage to the liver, pancreas, and heart organs, as well as Parkinson's and Alzheimer's diseases (Wechakorn et al., 2021). Therefore, speciation analysis of these ions is necessary.

In this study, the synthesized GL-AgNPs and GL-AuNPs were applied as a probe for the detection of metal ions in aqueous solutions. The selectivity of the GL-MNPs assay was tested with various environmentally important metal ions, such as Al^{3+}, Cr^{3+}, Fe^{3+}, Mn^{2+}, Zn^{2+}, Ni^{2+}, Mg^{2+}, Pb^{2+}, Ba^{2+}, Ca^{2+}, Cu^{2+}, and Fe^{2+}. The results revealed that GL-AuNPs were not sensitive to all testing metal ions at concentrations less than 1000 nM, so they were not studied further for sensing application. Meanwhile, AgNPs exhibited excellent sensitivity toward Fe^{3+} ions.

As shown in Fig. 4a, the addition of Al^{3+}, Cr^{3+}, Mn^{2+}, Zn^{2+}, Ni^{2+}, Mg^{2+}, Pb^{2+}, Ba^{2+}, Ca^{2+}, Cu^{2+}, and Fe^{2+} (100 nM) did not cause any evident change in the color and the SPR peak of the GL-AgNPs colloid. Upon interaction with Fe^{3+} ions, the SPR peak intensity decreased sharply, and the GL-AgNPs solution color changed from dark yellow to colorless. The remarkable selectivity of GL-AgNPs toward Fe^{3+} could be related to the high chelating ability of Fe^{3+} ions with biomolecules capping AgNPs. Therein, Fe^{3+} ions acted as a bridge linking GL-AgNPs together, causing agglomeration. Different concentrations of target ions can generate variable degrees of aggregation; and the variation in distance between the aggregated nanoparticles leads to the change of the SPR peak and the solution color. This is the general mechanism of the colorimetric detection of metals using biogenic AgNPs (Liu et al., 2020).

Further, the different concentrations of Fe^{3+} in the range of 0.1–500 nM were added to GL-AgNPs to establish a calibration curve, which can allow the quantification of Fe^{3+}. Fig. 4b depicts the change of the SPR intensity with the concentration of Fe^{3+}. Obviously, the absorbance of the SPR peak decreased as increasing Fe^{3+} concentration, probably due to the increased degree of aggregation of GL-AgNPs (Ratnarathorn et al., 2015). Besides, the slight shift of the SPR peak from 420 to 415 nm was also observed when Fe^{3+} ions were introduced. This phenomenon may be associated with chelate formation between Fe^{3+} and GL extract biomolecules wrapped AgNPs. The relative sensitivity plot of $(A_o - A)/A_o$ versus Fe^{3+} concentration (A_o and A are the SPR band absorbance of GL-AgNPs at zero and relative Fe^{3+} concentrations, respectively) was further built for the Fe^{3+} quantification, as presented in Fig. 4c. It can be seen that in the whole tested range of 0–500 nM, the relationship between the SPR absorption intensity and Fe^{3+} ion concentration was non-linear and can be expressed by the power model equation $(A_o - A)/A_o = 0.134x[Fe^{3+}]^{0.294}$ with a correlation coefficient (R^2) of 0.9921. Furthermore, a linear behavior of the relative sensitivity was found in a concentration range of 50–500 nM, which was described by the regression equation $(A_o - A)/A_o = 8.76x10^{-4}[Fe^{3+}] + 0.418$ with R^2 of 0.993. The sensitivity of the proposed method was evaluated by the LOD

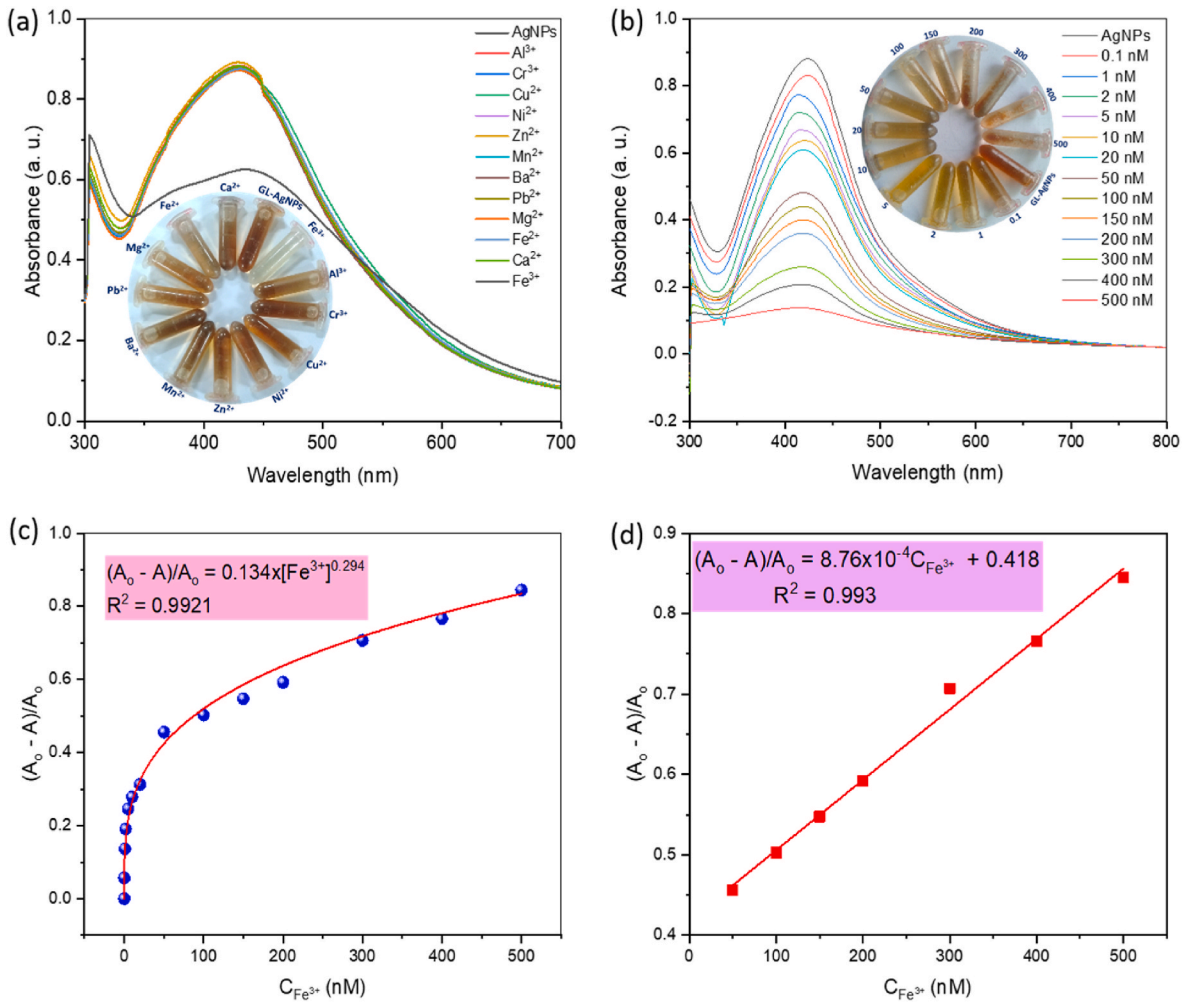

Fig. 4. UV–Vis spectra of GL-AgNPs incubated with various metal ions (a), with different Fe^{3+} concentrations (b), the plot of $(A_o - A)/A_o$ versus Fe^{3+} concentrations in a range of 0–500 nM (c) and 50–500 (d).

factor, which was determined based on the 3σ rule (where σ is the standard deviation of ten independent measurements of a blank sample). The calculated LOD for the GL-AgNPs sensor was 1.85 nM, which is much lower than the allowed Fe^{3+} concentration limit (5.36 μg/L) defined by the World Health Organization. Notably, compared with some other colorimetric assays listed in Table 1, the GL-AgNPs probe showed a considerably lower LOD value, proving the excellent sensitivity of the developed sensing system towards Fe^{3+}.

To validate the practicability of the offered method, five tap water samples spiked with stock Fe^{3+} solution (the final Fe^{3+} concentration of 75, 150, 350, and 450 nM) were analyzed by the GL-AgNPs probe and the AAS technique. The testing data are given in Table 2. From Table 2, it can be noticed that the results measured by GL-AgNPs were not significantly different from the standard AAS method. Moreover, the developed nanosensor exhibited satisfactory recoveries, varying in a range of 99.5–102.1%. The obtained results indicated that the present proposed assay is a promising method for the accurate determination of Fe^{3+} ions in real water.

Table 1
LOD values of some colorimetric assays for Fe^{3+} detection.

Materials	LOD (μM)	Linear range (μM)	Ref.
N-acetyl-L-cysteine- AgNPs	8.0	8–80	Gao et al. (2015)
Bauhinia variegate-AgNPs	2.08	6–100	Uzunoğlu et al. (2020)
Starch-coated AgNPs	1.8	12.5–125	Vasileva et al. (2019)
Poria cocos-AgNPs	1.5	0–250	(Le et al. 2021a, 2021b)
AuNPs@lactose/alginate	0.8	2.0–80	Ho et al. (2021)
Diaminodiphenyl sulfone-AuNPs	0.69	1.0–500	Meena et al. (2020)
Calix[4] resorcinarene polyhydrazide - AgNPs	0.1	0.1–10	Zhan et al. (2012)
GL-AgNPs	0.0185	0.05–0.5	This study

3.4. Antibacterial activity

The green-synthesized MNPs were further investigated for antibacterial activity against two Gram-negative (*E. coli,* and *P. aeruginosa*) and three Gram-positive strains (*B. subtilis*, *S. aureus,* and *B. cereus*) using the well diffusion method. The results (Fig. S3) revealed that GL-AuNPs did

Table 2
Determination of Fe^{3+} concentration in tap water by AAS and GL-AgNPs probe.

Spiked concentration (nM)	Determined concentration (nM)		Recovery (%)
	AAS	GL-AgNPs assay	
75	75.8 ± 1.2	76.6 ± 1.6	102.1
150	151.1 ± 0.9	151.7 ± 0.7	101.1
350	350.8 ± 1.7	349.1 ± 1.2	99.7
450	449.2 ± 2.1	447.9 ± 1.8	99.5

not exhibit antibacterial activity against all the tested bacterial strains in the range of the examined concentrations. The same phenomenon was reported for several plant-mediated AuNPs (Reddy et al., 2017; Doan et al., 2020a; Vo et al., 2019). The exact reason for this situation is still not clearly explored. It has been suggested that the low inhibition activity of AuNPs could be related to their inertness and the thickness of the organic capped layer. In the case of GL-AuNPs, the organic layer surrounding them was too thick (as determined by DLS), which prevented physical contact with the bacteria, reducing the antibacterial performance. Meanwhile, GL-AgNPs exhibited a strong inhibition efficiency toward all the tested bacterial strains, as displayed in Fig. 5. The antibacterial activity of the tested samples was assessed by the formation of an inhibition zone around the well. The diameters of the zones of inhibition for the tested bacteria were presented in Fig. 6. It is clear that the size of zones of inhibition for all pathogenic bacteria slightly increased with raising the concentration of GL-AgNPs. The antibacterial effect of GL-AgNPs at the highest concentration (160 ppm) was almost equivalent to that of the gentamicin antibiotic. Meantime, GL extract showed very low antibacterial activity. The highest growth inhibition activity of GL-AgNPs was observed against *B. subtilis* (14.58 ± 0.35 mm), followed by *B. cereus* (13.8 ± 0.52 mm), *P. aeruginosa* (12.38 ± 0.64 mm), *E. coli* (11.3 ± 0.72 mm), and *S. aureus* (10.41 ± 0.31 mm). More importantly, GL-AgNPs also showed competitive antibacterial activity with AgNPs synthesized from extracts of other plants listed in Table 3. Therefore, with the high antimicrobial effect, GL-AgNPs can potentially be employed as an effective antibacterial agent in environmental, biotechnological and biomedical applications.

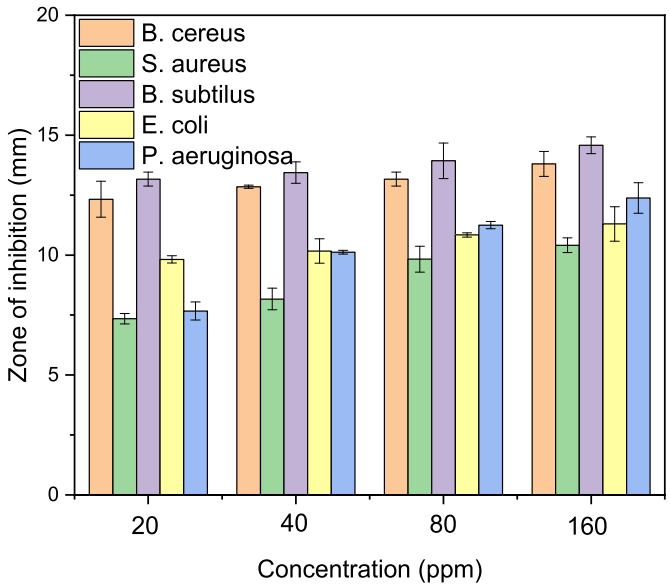

Fig. 6. Zone of inhibition of GL-AgNPs against different bacterial strains.

4. Conclusions

The present study demonstrated the green-synthesis of AgNPs and AuNPs using *Ganoderma lucidum* mushroom extract as reducing and capping agents. The morphological, structural, optical, catalytic and antimicrobial properties of the biosynthesized MNPs were investigated. GL-AgNPs and GL-AuNPs possessed the face-centered cubic structure with high crystalline nature. The TEM analysis confirmed the spherical morphology of GL-AgNPs crystals with an average diameter of about 50 nm and the multi-shaped structures of GL-AuNPs with grain sizes of 15–40 nm. Both GL-AgNPs and GL-AuNPs manifested excellent catalytic activity for the reduction of 4-NP to 4-AP by $NaBH_4$; the conversion efficiency reached more than 98% in 9 min and was maintained higher than 95% after five reuses. GL-AgNPs offered high selectivity and sensitivity towards Fe^{3+} with a low LOD of 1.85 nM. The tests in tap water samples further confirmed a high potential of the practical

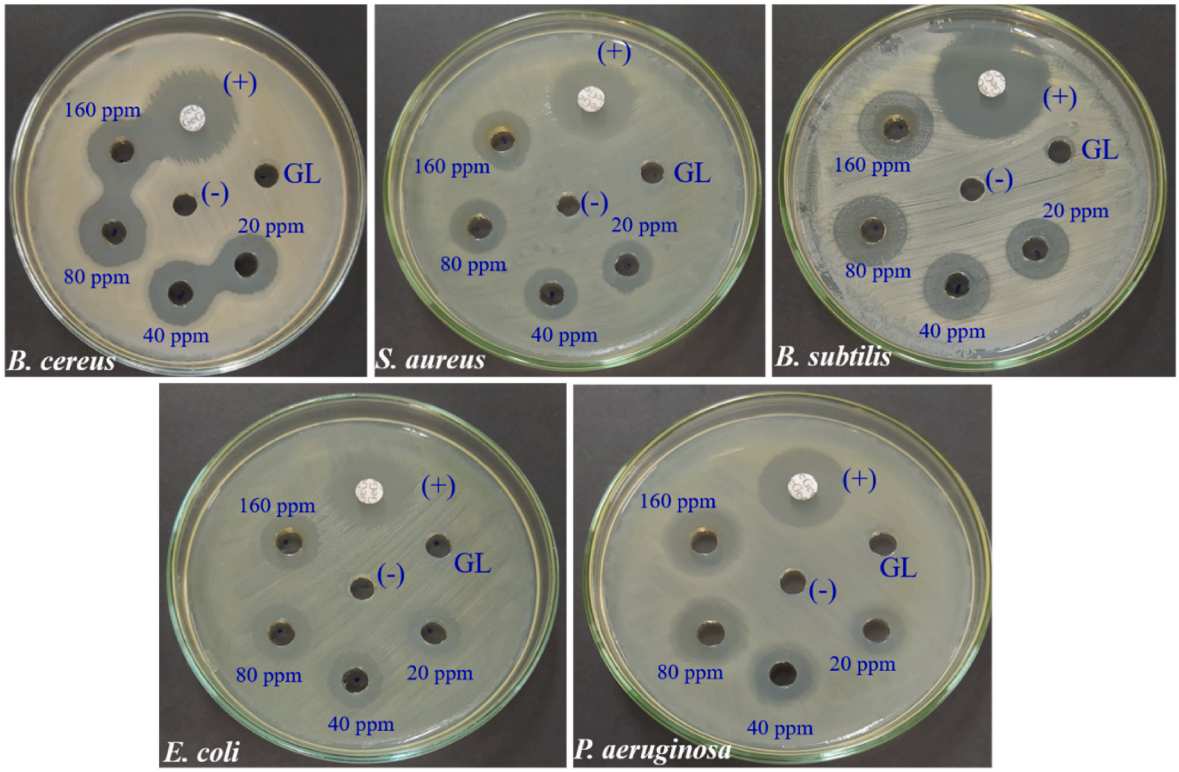

Fig. 5. Antibacterial activity of GL-AgNPs against *B. cereus*, *S. aureus*, *B.subtilus*, *E. coli*, and *P. aeruginosa* with different concentrations. (+): Gentamicin antibiotic, (−): sterile distilled water, GL: *Ganoderma lucidum* extract.

Table 3
Comparison of antibacterial activity of some plant-mediated AgNPs.

Bacterial strains	Plant resources	AgNPs size (nm)	Concentration of AgNPs (ppm)	Zone of inhibition (mm)	Ref.
B. cereus	Urtica dioica	20–30	500	14	Jyoti et al. (2016)
	Parkia speciosa	35	100	5.0	Ravichandran et al. (2019)
	Codonopsis pilosula	10	80	12.0 ± 0.85	Doan et al. (2020a)
	Ganoderma lucidum	50	20	12.33 ± 0.75	This study
S. aureus	*Capsella bursa-pastoris*	16.2 ± 8.4	216	10.78 ± 0.23	Salayová et al. (2021a)
	Parkia speciosa	35	100	10.0	Ravichandran et al. (2019)
	Codonopsis pilosula	10	80	17.0 ± 1.2	Doan et al. (2020a)
	Ganoderma lucidum	50	20	7.35 ± 0.22	This study
B. subtilis	Mukia maderaspatana	58	1000	11 ± 0.05	Harshiny et al. (2015)
	Terminalia chebula	22	20	6	Ankegowda et al. (2020)
	Pedalium murex	20–50	16.2	10	Anandalakshmi et al. (2016a)
	Ganoderma lucidum	50	20	13.17 ± 0.29	This study
E. coli	Capsella bursa-pastoris	16.2 ± 8.4	216	9.30 ± 0.23	(Salayová et al., 2021a)
	Parkia speciosa	35	100	9.0	Ravichandran et al. (2019)
	Codonopsis pilosula	10	80	7.0 ± 0.42	Doan et al. (2020a)
	Ganoderma lucidum	50	20	9.82 ± 0.15	This study
P. aeruginosa	Capsella bursa-pastoris	16.2 ± 8.4	216	11.80 ± 2.01	(Salayová et al., 2021a)
	Skimmia laureola	38 ± 0.27	10	14.33	Ahmed et al. (2015)
	Pedalium murex	20–50	16.2	10.5	Anandalakshmi et al. (2016b)
	Ganoderma lucidum	50	20	7.67 ± 0.38	This study

application of the GL-AgNP based nanosensor for detection of Fe^{3+} ions in real water systems. Besides, GL-AgNPs also showed strong antibacterial activity against several bacterial strains, including *E. coli, P. aeruginosa, B. subtilis*, *S. aureus,* and *B. cereus*. The difference in thickness of the protective organic layer and particle sizes may be the reason why GL-AgNPs possess more outstanding properties than those of GL-AuNPs in environmental, catalytic and biotechnological applications.

Credit author statement

Thi Hong Anh Nguyen: Conceptualization, Writing – original draft, Investigation. **Van-Cuong Nguyen**: Software, Investigation, Data curation. **Thi Nhu Huynh Phan**: Resources, Methodology, Investigation. **Van Thuan Le:** Methodology, Supervision, Editing, and Final revisions. **Yasser Vasseghian**: Reviewing, Investigation, Software, Visualization. **Mikhail Alexandrovich Trubitsyn**: Data curation, Validation. **Anh-Tien Nguyen:** Conceptualization, Formal analysis**. Tan Phat Chau:** Formal analysis, Methodology, Software**. Van-Dat Doan**: Writing - review & editing, Supervision.

Declaration of competing interest

The authors declare that they have no known competing financial interests or personal relationships that could have appeared to influence the work reported in this paper.

Appendix A. Supplementary data

Supplementary data to this article can be found online at https://doi.org/10.1016/j.chemosphere.2021.132271.

References

Ahmed, M.J., Murtaza, G., Mehmood, A., Bhatti, T.M., 2015. Green synthesis of silver nanoparticles using leaves extract of Skimmia laureola: characterization and antibacterial activity. Mater. Lett. 153, 10–13. https://doi.org/10.1016/J.MATLET.2015.03.143.

Ajitha, B., Ashok Kumar Reddy, Y., Reddy, P.S., 2014. Biogenic nano-scale silver particles by Tephrosia purpurea leaf extract and their inborn antimicrobial activity. Spectrochim. Acta Part A Mol. Biomol. Spectrosc. 121, 164–172. https://doi.org/10.1016/j.saa.2013.10.077.

Al-Ansari, M.M., Dhasarathan, P., Ranjitsingh, A.J.A., Al-Humaid, L.A., 2020. Ganoderma lucidum inspired silver nanoparticles and its biomedical applications with special reference to drug resistant Escherichia coli isolates from CAUTI. Saudi J. Biol. Sci. 27, 2993–3002. https://doi.org/10.1016/J.SJBS.2020.09.008.

Alavi, M., Rai, M., 2019. Recent advances in antibacterial applications of metal nanoparticles (MNPs) and metal nanocomposites (MNCs) against multidrug-resistant (MDR) bacteria. Expert Rev. Anti Infect. Ther. 17, 419–428. https://doi.org/10.1080/14787210.2019.1614914.

Albukhari, S.M., Ismail, M., Akhtar, K., Danish, E.Y., 2019. Catalytic reduction of nitrophenols and dyes using silver nanoparticles @ cellulose polymer paper for the resolution of waste water treatment challenges. Colloids Surfaces A Physicochem. Eng. Asp. 577, 548–561. https://doi.org/10.1016/j.colsurfa.2019.05.058.

Anandalakshmi, K., Venugobal, J., Ramasamy, V., 2016a. Characterization of silver nanoparticles by green synthesis method using Pedalium murex leaf extract and their antibacterial activity. Appl. Nanosci. 6, 399–408. https://doi.org/10.1007/s13204-015-0449-z.

Anandalakshmi, K., Venugobal, J., Ramasamy, V., 2016b. Characterization of silver nanoparticles by green synthesis method using Pedalium murex leaf extract and their antibacterial activity. Appl. Nanosci. 6, 399–408. https://doi.org/10.1007/s13204-015-0449-z.

S., R.P. Ankegowda, V.M., Kollur, S.P., Prasad, S.K., Pradeep, S., Dhramashekara, C., Jain, A.S., Prasad, A., Srinivasa, C., Sridhara Setty, P.B., Gopinath, S.M., Bahkali, A. H., Syed, A., Shivamallu, C., 2020. Phyto-mediated synthesis of silver nanoparticles using Terminalia chebula fruit extract and evaluation of its cytotoxic and antimicrobial potential Molecules 25, 5042. https://doi.org/10.3390/molecules25215042.

Behzad, F., Naghib, S.M., Kouhbanani, M.A.J., Tabatabaei, S.N., Zare, Y., Rhee, K.Y., 2021. An overview of the plant-mediated green synthesis of noble metal nanoparticles for antibacterial applications. J. Ind. Eng. Chem. 94, 92–104. https://doi.org/10.1016/j.jiec.2020.12.005.

Berahim, N., Basirun, W.J., Leo, B.F., Johan, M.R., 2018. Synthesis of bimetallic gold-silver (Au-Ag) nanoparticles for the catalytic reduction of 4-nitrophenol to 4-aminophenol. Catalysts 8. https://doi.org/10.3390/catal18100412.

Buledi, J.A., Amin, S., Haider, S.I., Bhanger, M.I., Solangi, A.R., 2020. A review on detection of heavy metals from aqueous media using nanomaterial-based sensors. Environ. Sci. Pollut. Res. https://doi.org/10.1007/s11356-020-07865-7.

Dao, M.U., Le, H.S., Hoang, H.Y., Tran, V.A., Doan, V.D., Le, T.T.N., Sirotkin, A., Le, V.T., 2020. Natural core-shell structure activated carbon beads derived from Litsea glutinosa seeds for removal of methylene blue: facile preparation, characterization, and adsorption properties. Environ. Res. 110481 https://doi.org/10.1016/j.envres.2020.110481.

Doan, V.-D., Huynh, B.-A., Nguyen, T.-D., Cao, X.-T., Nguyen, V.-C., Nguyen, T.L.-H., Nguyen, H.T., Le, V.T., 2020a. Biosynthesis of silver and gold nanoparticles using aqueous extract of Codonopsis pilosula roots for antibacterial and catalytic applications. J. Nanomater. 2020, 1–18. https://doi.org/10.1155/2020/8492016.

Doan, V.-D., Thieu, A.T., Nguyen, T.-D., Nguyen, V.-C., Cao, X.-T., Nguyen, T.L.-H., Le, V. T., 2020b. Biosynthesis of gold nanoparticles using Litsea cubeba fruit extract for catalytic reduction of 4-nitrophenol. J. Nanomater. 2020, 1–10. https://doi.org/10.1155/2020/4548790.

Doan, V.D., Nguyen, N.V., Nguyen, T.L.H., Tran, V.A., Le, V.T., 2021. High-efficient reduction of methylene blue and 4-nitrophenol by silver nanoparticles embedded in magnetic graphene oxide. Environ. Sci. Pollut. Res. https://doi.org/10.1007/s11356-021-13597-z.

Gangapuram, B.R., Bandi, R., Alle, M., Dadigala, R., Kotu, G.M., Guttena, V., 2018. Microwave assisted rapid green synthesis of gold nanoparticles using Annona squamosa L peel extract for the efficient catalytic reduction of organic pollutants. J. Mol. Struct. 1167, 305–315. https://doi.org/10.1016/j.molstruc.2018.05.004.

Gao, X., Lu, Y., He, S., Li, X., Chen, W., 2015. Colorimetric detection of iron ions (III) based on the highly sensitive plasmonic response of the N-acetyl-l-cysteine-stabilized silver nanoparticles. Anal. Chim. Acta 879, 118–125. https://doi.org/10.1016/j.aca.2015.04.002.

Grzeschik, R., Schäfer, D., Holtum, T., Küpper, S., Hoffmann, A., Schlücker, S., 2020. On the overlooked critical role of the pH value on the kinetics of the 4-nitrophenol

NaBH 4 -reduction catalyzed by noble-metal nanoparticles (Pt, Pd, and Au). J. Phys. Chem. C 124. https://doi.org/10.1021/acs.jpcc.9b07114.
Harshiny, M., Matheswaran, M., Arthanareeswaran, G., Kumaran, S., Rajasree, S., 2015. Enhancement of antibacterial properties of silver nanoparticles–ceftriaxone conjugate through Mukia maderaspatana leaf extract mediated synthesis. Ecotoxicol. Environ. Saf. 121, 135–141. https://doi.org/10.1016/j.ecoenv.2015.04.041.
Hassan, S.S., Carlson, K., Mohanty, S.K., Sirajuddin Canlier, A., 2018. Ultra-rapid catalytic degradation of 4-nitrophenol with ionic liquid recoverable and reusable ibuprofen derived silver nanoparticles. Environ. Pollut. 237, 731–739. https://doi.org/10.1016/j.envpol.2017.10.118.
Ho, T.T.-T., Dang, C.-H., Huynh, T.K.-C., Hoang, T.K.-D., Nguyen, T.-D., 2021. In situ synthesis of gold nanoparticles on novel nanocomposite lactose/alginate: recyclable catalysis and colorimetric detection of Fe(III). Carbohydr. Polym. 251, 116998. https://doi.org/10.1016/j.carbpol.2020.116998.
Jyoti, K., Baunthiyal, M., Singh, A., 2016. Characterization of silver nanoparticles synthesized using Urtica dioica Linn. leaves and their synergistic effects with antibiotics. J. Radiat. Res. Appl. Sci. 9, 217–227. https://doi.org/10.1016/j.jrras.2015.10.002.
Karst, P., 2020. Traditional Uses , Chemical Components and 42084–42097. https://doi.org/10.1039/d0ra07219b.
Le, V.T., Ngu, N.N.Q., Chau, T.P., Nguyen, T.D., Nguyen, V.T., Nguyen, T.L.H., Cao, X.T., Doan, V., 2021a. Silver and gold nanoparticles from *Limnophila rugosa* leaves: biosynthesis, characterization, and catalytic activity in reduction of nitrophenols. J. Nanomater. 2021, 1–11. https://doi.org/10.1155/2021/5571663.
Le, V.T., Nguyen, V.-C., Cao, X., Chau, T.P., Nguyen, T.D., Nguyen, T.L., Doan, V., 2021b. Highly effective degradation of nitrophenols by biometal nanoparticles synthesized using *Caulis spatholobi* extract. J. Nanomater. 2021, 1–11. https://doi.org/10.1155/2021/6696995.
Le, Van Thuan, Duong, T.G., Le, Van Tan, Phan, T.L., Huong Nguyen, T.L., Chau, T.P., Doan, V.D., 2021. Effective reduction of nitrophenols and colorimetric detection of Pb(II) ions by: *Siraitia grosvenorii* fruit extract capped gold nanoparticles. RSC Adv 11, 15438–15448. https://doi.org/10.1039/d1ra01593a.
Liu, B., Zhuang, J., Wei, G., 2020. Recent advances in the design of colorimetric sensors for environmental monitoring. Environ. Sci. Nano 7, 2195–2213. https://doi.org/10.1039/D0EN00449A.
Meena, R., Mehta, V.N., Bhamore, J.R., Rao, P.T., Park, T.J., Kailasa, S.K., 2020. Diaminodiphenyl sulfone as a novel ligand for synthesis of gold nanoparticles for simultaneous colorimetric assay of three trivalent metal cations (Al^{3+}, Fe^{3+} and Cr^{3+}). J. Mol. Liq. 312, 113409. https://doi.org/10.1016/J.MOLLIQ.2020.113409.
Modrzejewska-Sikorska, A., Konował, E., 2020. Silver and gold nanoparticles as chemical probes of the presence of heavy metal ions. J. Mol. Liq. 302 https://doi.org/10.1016/j.molliq.2020.112559.
My-Thao Nguyen, T., Anh-Thu Nguyen, T., Tuong-Van Pham, N., Ly, Q.V., Thuy-Quynh Tran, T., Thach, T.D., Nguyen, C.L., Banh, K.S., Le, V.D., Nguyen, L.P., Nguyen, D.T., Dang, C.H., Nguyen, T.D., 2021. Biosynthesis of metallic nanoparticles from waste Passiflora edulis peels for their antibacterial effect and catalytic activity. Arab. J. Chem. 14, 103096. https://doi.org/10.1016/j.arabjc.2021.103096.
Nayak, S., Sajankila, S.P., Rao, C.V., 2018. Green synthesis of gold nanoparticles from banana pith extract and its evaluation of antibacterial activity and catalytic reduction of Malachite green dye. J. Microbiol. Biotechnol. Food Sci. 7, 641–645. https://doi.org/10.15414/jmbfs.2018.7.6.641-645.
Rarima, R., Unnikrishnan, G., 2020. Porous poly(lactic acid)/nano-silver composite membranes for catalytic reduction of 4-nitrophenol. Mater. Chem. Phys. 241, 122389. https://doi.org/10.1016/j.matchemphys.2019.122389.
Ratnarathorn, N., Chailapakul, O., Dungchai, W., 2015. Highly sensitive colorimetric detection of lead using maleic acid functionalized gold nanoparticles. Talanta 132, 613–618. https://doi.org/10.1016/j.talanta.2014.10.024.
Ravichandran, V., Vasanthi, S., Shalini, S., Shah, S.A.A., Tripathy, M., Paliwal, N., 2019. Green synthesis, characterization, antibacterial, antioxidant and photocatalytic activity of *Parkia speciosa* leaves extract mediated silver nanoparticles. Results Phys 15, 102565. https://doi.org/10.1016/j.rinp.2019.102565.
Reddy, B.P., Mallikarjuna, K., Narasimha, G., Park, S., 2017. *Plectranthus amboinicus*-mediated silver, gold, and silver-gold nanoparticles: phyto-synthetic, catalytic, and antibacterial studies. Mater. Res. Express 4, 085010. https://doi.org/10.1088/2053-1591/aa80a2.
Salayova, A., Bedlovicova, Z., Daneu, N., Balaz, M., Lukacova Bujnakova, Z., Balazova, Ľ., Tkacikova, Ľ., 2021. Green synthesis of silver nanoparticles with antibacterial activity using various medicinal plant extracts: morphology and antibacterial efficacy. Nanomaterials 11, 1005. https://doi.org/10.3390/nano11041005.
Saravanan, A., Kumar, P.S., Karishma, S., Vo, D.V.N., Jeevanantham, S., Yaashikaa, P.R., George, C.S., 2021. A review on biosynthesis of metal nanoparticles and its environmental applications. Chemosphere 264, 128580. https://doi.org/10.1016/J.CHEMOSPHERE.2020.128580.
Seku, K., Gangapuram, B.R., Pejjai, B., Kadimpati, K.K., Golla, N., 2018. Microwave-assisted synthesis of silver nanoparticles and their application in catalytic, antibacterial and antioxidant activities. J. Nanostructure Chem. 8, 179–188. https://doi.org/10.1007/s40097-018-0264-7.
Shimoga, G., Palem, R.R., Lee, S., Kim, S., 2020. Catalytic degradability of p-nitrophenol using ecofriendly silver nanoparticles. Metals 10, 1661. https://doi.org/10.3390/met10121661.
Soni, V., Raizada, P., Singh, P., Cuong, H.N., S, R., Saini, A., Saini, R.V., Le, Q. Van, Nadda, A.K., Le, T.-T., Nguyen, V.-H., 2021. Sustainable and green trends in using plant extracts for the synthesis of biogenic metal nanoparticles toward environmental and pharmaceutical advances: a review. Environ. Res. 202, 111622. https://doi.org/10.1016/J.ENVRES.2021.111622.
Thi Thanh Nhi, L., Van Thuan, L., My Uyen, D., Nguyen, M.H., Thu, V.T., Khieu, D.Q., Sinh, L.H., 2020. Facile fabrication of highly flexible and floatable Cu_2O/rGO on Vietnamese traditional paper toward high-performance solar-light-driven photocatalytic degradation of ciprofloxacin antibiotic. RSC Adv 10, 16330–16338. https://doi.org/10.1039/D0RA01854F.
Uzunoğlu, D., Ergüt, M., Kodaman, C.G., Özer, A., 2020. Biosynthesized silver nanoparticles for colorimetric detection of Fe^{3+} ions. Arabian J. Sci. Eng. https://doi.org/10.1007/s13369-020-04760-8.
Vasileva, P., Dobrev, S., Karadjova, I., 2019. Colorimetric detection of iron(III) based on sensitive and selective plasmonic response of starch-coated silver nanoparticles. Proc.SPIE.
Vo, T.-T., Dang, C.-H., Doan, V.-D., Dang, V.-S., Nguyen, T.-D., 2020. Biogenic synthesis of silver and gold nanoparticles from *Lactuca indica* leaf extract and their application in catalytic degradation of toxic compounds. J. Inorg. Organomet. Polym. Mater. 30, 388–399. https://doi.org/10.1007/s10904-019-01197-x.
Vo, T.-T., Nguyen, Thi Thanh-Ngan, Huynh, T.T.-T., Vo, T.T.-T., Nguyen, Thi Thuy-Nhung, Nguyen, D.-T., Dang, V.-S., Dang, C.-H., Nguyen, T.-D., 2019. Biosynthesis of silver and gold nanoparticles using aqueous extract from *Crinum latifolium* leaf and their applications forward antibacterial effect and wastewater treatment. J. Nanomater. 1–14. https://doi.org/10.1155/2019/8385935.
Wechakorn, K., Chomngam, S., Eiamprasert, U., Kongsaeree, P., 2021. A rhodamine–bistriazole based fluorescent and colorimetric sensor containing a phenyl linker for Fe(III) detection. Chem. Pap. 75, 883–892. https://doi.org/10.1007/s11696-020-01349-1.
Xu, Y., Shi, X., Hua, R., Zhang, R., Yao, Y., Zhao, B., Liu, T., Zheng, J., Lu, G., 2020. Remarkably catalytic activity in reduction of 4-nitrophenol and methylene blue by Fe_3O_4@COF supported noble metal nanoparticles. Appl. Catal. B Environ. 260, 118142. https://doi.org/10.1016/j.apcatb.2019.118142.
Yu, C., Tang, J., Liu, X., Ren, X., Zhen, M., Wang, L., 2019. Green biosynthesis of silver nanoparticles using Eriobotrya japonica (thunb.) leaf extract for reductive catalysis. Materials 12. https://doi.org/10.3390/ma12010189.
Zhan, J., Wen, L., Miao, F., Tian, D., Zhu, X., Li, H., 2012. Synthesis of a pyridyl-appended calix[4]arene and its application to the modification of silver nanoparticles as an Fe^{3+} colorimetric sensor. New J. Chem. 36, 656–661. https://doi.org/10.1039/c2nj20776a.